AFRL-RH-WP-TR-2022-0090

EXTRACELLULAR RNA: NOVEL BIOMARKER AND POTENTIAL THERAPEUTIC TARGET IN TRAUMA

Wei Chao

Center for Shock, Trauma and Anesthesiology Research
University of Maryland School of Medicine

MAY 2022
Final Report

AIR FORCE RESEARCH LABORATORY
711TH HUMAN PERFORMANCE WING,
AIRMAN SYSTEMS DIRECTORATE,
WRIGHT-PATTERSON AIR FORCE BASE, OH 45433
AIR FORCE MATERIEL COMMAND
UNITED STATES AIR FORCE

NOTICE AND SIGNATURE PAGE

Using Government drawings, specifications, or other data included in this document for any purpose other than Government procurement does not in any way obligate the U.S. Government. The fact that the Government formulated or supplied the drawings, specifications, or other data does not license the holder or any other person or corporation; or convey any rights or permission to manufacture, use, or sell any patented invention that may relate to them.

This report was cleared for public release by the Air Force Research Laboratory Public Affairs Office and is available to the general public, including foreign nationals. Copies may be obtained from the Defense Technical Information Center (DTIC) (http://www.dtic.mil).

AFRL-RH-WP-TR-2022-0090 HAS BEEN REVIEWED AND IS APPROVED FOR PUBLICATION IN ACCORDANCE WITH ASSIGNED DISTRIBUTION STATEMENT.

BURKE.ALICIA.N.1125850452 Digitally signed by BURKE.ALICIA.N.1125850452 Date: 2023.02.21 10:11:14 -05'00'

ALICIA BURKE
Program Manager
Product Development Branch
Airman Biosciences Division

DALTON.MATTHEW.J.1291876460 Digitally signed by DALTON.MATTHEW.J.1291876460 Date: 2023.02.23 08:20:40 -05'00'

MATTHEW DALTON, DR-III
Product Area Lead, En Route Care Section
Product Development Branch
Airman Biosciences Division

This report is published in the interest of scientific and technical information exchange, and its publication does not constitute the Government's approval or disapproval of its ideas or findings.

REPORT DOCUMENTATION PAGE

Form Approved
OMB No. 0704-0188

1. REPORT DATE *(DD-MM-YY)*	2. REPORT TYPE	3. DATES COVERED *(From - To)*
20-05-22	Final	01 Feb 2017 – 20 May 2022

4. TITLE AND SUBTITLE
Extracellular RNA: Novel Biomarker and Potential Therapeutic Target in Trauma

5a. CONTRACT NUMBER
FA8650-17-2-6H12

5b. GRANT NUMBER

5c. PROGRAM ELEMENT NUMBER

6. AUTHOR(S)
Wei Chao

5d. PROJECT NUMBER

5e. TASK NUMBER

5f. WORK UNIT NUMBER
Legacy

7. PERFORMING ORGANIZATION NAME(S) AND ADDRESS(ES)
University of Maryland, Baltimore
620 W. Lexington Street, 4th floor
Baltimore, Maryland 21201

8. PERFORMING ORGANIZATION REPORT NUMBER

9. SPONSORING/MONITORING AGENCY NAME(S) AND ADDRESS(ES)
Air Force Materiel Command
Air Force Research Laboratory
711th Human Performance Wing
Airman Systems Directorate
Airman Biosciences Division
Product Development Branch
Wright-Patterson AFB, OH 45433

10. SPONSORING/MONITORING AGENCY ACRONYM(S)
711 HPW/RHBA

11. SPONSORING/MONITORING AGENCY REPORT NUMBER(S)
AFRL-RH-WP-TR-2022-0090

12. DISTRIBUTION/AVAILABILITY STATEMENT
Distribution A: Approved for public release.

13. SUPPLEMENTARY NOTES
AFRL-2022-5992, cleared 11 January 2023

14. ABSTRACT
Traumatic injury is a major cause of combat casualty and modality. Trauma can induce profound systemic inflammatory responses and multiple remote organ damage. While the clinical manifestations/courses of traumatic injury have been well described, the molecular mechanism leading to inflammation and organ failure is poorly understood. Moreover, rapid aeromedical evacuation has been used in battlefield to save lives, but also has subjected warfighters to hypobaric conditions. How hypobaric conditions impact the body's immune system and its response to traumatic injury is unclear. In this report, we highlight several important findings in an animal model of polytrauma: 1) Plasma RNA from traumatic animals may drive and amplify systemic inflammation and contribute to remote organ injury; 2) RNA sequencing and in vitro/in vivo assays identified a group of plasma miRNAs that may function as inflammatory driver and contribute to organ injury; and finally, 3) Hypobaric exposure worsens endothelial injury and cardiac contractile dysfunction. These findings suggest that hypobaria may represent a "second hit" following initial traumatic injury and during aeromedical evacuation, high-altitude hypobaric exposure even with adequate oxygen supply may impose harmful effects after traumatic injury.

15. SUBJECT TERMS
trauma; injury; extracellular RNA; microRNA; innate immunity; toll-like receptor

16. SECURITY CLASSIFICATION OF:			17. LIMITATION OF ABSTRACT:	18. NUMBER OF PAGES	19a. NAME OF RESPONSIBLE PERSON (Monitor)
a. REPORT	b. ABSTRACT	c. THIS PAGE			Alicia Burke
Unclassified	Unclassified	Unclassified	SAR	29	19b. TELEPHONE NUMBER *(Include Area Code)* N/A

TABLE OF CONTENTS

Page

LIST OF FIGURES

Page

LIST OF TABLES

Page

1.0 EXECUTIVE SUMMARY

Traumatic injury is a major cause of combat casualty and modality. In additional to direct traumatic injury to the impact body parts, trauma can also induces profound systemic inflammatory responses and multiple remote organ damage such as liver, lung, heart, and kideny. While the clinical manifestations/courses of traumatic injury have been well described, the molecular mechanism responsible for systemic inflammatory injury and organ failure in traumatic patients is not completely understood. Moreover, rapid aeromedical evacuation (AE) has been used in battle field to save lives, but also has subjected war fighters to hypobaric and hypoxic conditions. While extensive research has been done investigating the impact of AE on traumatic brain injury (TBI), how hypobaric/hypoxic conditions impact the body's innate and active immune system and its response to traumatic injury is unclear. This project was designed to investigate 1) the role of circulating plasma Micro ribonucleic acid (miRNAs), a recently identified innate immune activator, in systemic inflammation and organ injury in an animal model of polytrauma (bowel ischemia, muscle crush, and bone fracture) and 2) the impact of hypobaric condition on systemic innate immune response and injury following traumatic injury. In the present study, we made several important findings. First, we discovered that plasma ribonucleic acid (RNA), released from tissues upon polytrauma, may drive and amplify systemic inflammation and contribute to remote organ injury. Second, RNA sequencing and in vitro/in vivo assays identified a group of plasma miRNAs that may function as important drivers in inflammatory storm and organ injury in trauma animals and these miRNAs work through innate immune receptor Toll-like receptor 7 (TLR7). Third, we found that ypobaria exposure worsens endothelial injury and cardiac contractile dysfunction. These findings suggest that hypobaria may represent a "second hit" following initial traumatic injury and during AE, high-altitude hypobaric exposure even with adequate oxygen supply may impose harmful effects after traumatic injury.

2.0 INTRODUCTION

Traumatic injury is a major cause of combat casualty and modality. Traumatic tissue injury rapidly activates the innate immune system and induces profound systemic hyper-inflammatory responses. These systemic hyper-inflammatory responses can cause severe collateral damage to the body, by leading to profound hemodynamic instability, tissue hypoxia, metabolic dysfunction, organ failure, and ultimately death. However, the mechanisms leading to immunological activation and organ failure after traumatic injury are unclear. Moreover, rapid AE has been used in battle field to save lives, but also has subjected war fighters to hypobaric and hypoxic conditions. While extensive research has been done investigating the impact of AE on TBI, how hypobaric/hypoxic conditions impact the body's innate and active immune system and its response to traumatic injury is unclear.

Micro ribonucleic acids (miRNA) are a group of small and single-stranded noncoding RNAs. While the primary role of miRNAs is to regulate gene expression, recent studies, including those from our laboratory, have suggested that miRNAs in the extracellular space may act on neighboring cells and play a role in various pathological conditions[1], including cancer metastasis[2], neurodegeneration[3], pain[4], and septic shock[5]. Injured tissues release *danger molecules* that can induce significant damage to tissues and organs in response to severe stress and insults, such as traumatic injury, shock, and ischemia-reperfusion injury. We were among the first to demonstrate that tissue RNA and microRNA are released into the circulation in response to hypoxic stress and/or septic shock and that extracellular microRNAs (ex-miRNA) exhibit potent proinflammatory properties and strongly activate the innate immune system both *in vitro* and *in vivo*[6-9] and may play a role in various organ injury and coagulopathy during septic shock[5, 10-12]. Moreover, there is a close correlation between the severity of shock and plasma RNA levels[5, 13]. These studies suggest that circulating miRNAs are danger molecules released from damaged tissues and may play an important role in systemic inflammation and organ injury in response to hypoxia and shock.

This final report highlights the results from an experimental project supported by the United States Air Force (2017-2020) that sought to investigate the role of circulating miRNAs in systemic inflammation and organ injury in an animal model of polytrauma and, furthermore, to define the impact of hypobaric condition on systemic innate immune response and injury following traumatic injury. The results described herein provide a fundamental understanding of the pathogenesis of polytraumatic injuries, such as those present in warfighter populations.

3.0 METHODS

3.1 Animals

Eight- to 12-week old sex- and age-matched wild type (WT) C57BL/6J mice were purchased from Jackson Laboratories (Bar Harbor, ME). $TLR3^{-/-}$ and $TLR7^{-/-}$ mice were originally purchased from Jackson Laboratories and have been bred in house for more than 10 generations. All animals were housed for at least one week before experiments in an air-conditioned, pathogen-free environment with free access to water and a bacteria-free diet at the Animal Veterinary Facilities at the University of Maryland School of Medicine. Blinding and randomization was conducted using simple sequential numbering generated manually to determine group assignment. All animal care and procedures were reviewed and approved by the Institutional Animal Care and Use Committee (IACUC) of the University of Maryland School of Medicine and comply with the "Guide for the Care and Use of Laboratory Animals" published by the National Institutes of Health. Importantly, all animal study protocols were reviewed and approved by the University of Maryland IACUC and approved by Air Force Research Laboratory (AFRL).

3.2 Murine model of polytrauma

A murine model of polytrauma was created consisting of bowel ischemia, bone fracture, and muscle crush, simulating combat injury such as those induced by improvised explosion device(s) (IEDs) (Figure (**Fig.) 1**). Male mice were anesthetized using isoflurane (3-4 percent (%) for induction, 1-3% for maintenance) with FIO2 of 95-97% at a flow rate of 100 millimeters per minute (mL/min). After midline laparotomy, the superior mesenteric artery (SMA) was exposed via a peri-hepatic approach and occluded at the aortic origin using a microvascular clip. Bowel ischemia was confirmed visually by pallor in the distal bowel, hyperperistalsis, and the absence of distal pulsating flow (**Fig. 1A**). The abdominal contents were replaced and the abdominal wall temporarily closed using Steri-Strips (3M, St Paul, MN) to minimize evaporative losses. Following 40 minutes (min) of bowel ischemia, the SMA was partially re-exposed and reperfusion was initiated by removal of the surgical clip and confirmed by the plethoric appearance of bowel indicating restoration of perfusion. The trauma model led to a marked systemic inflammation as evidenced by marked elevation of plasma Interleukin-6 (IL-6) (**Fig. 1B**). At the onset of SMA clipping, a unilateral midshaft tibia fracture was induced by blunt force and the ipsilateral gastrocnemius muscle crushed by application of a Kelly forceps for 30 min. Reduction and external fixation of the fracture was performed using tape splinting and a hollow foam boot cast (**Fig. 1C**). Sham animals underwent laparotomy and exposure of the SMA only. Fascial and skin layers were closed with running suture at the end of the sham or polytrauma procedures, and bupivacaine (3.5 milligrams per kilograms (mg/kg)). was infiltrated widely at the incision. All animals were maintained at 37°C using homeothermic heating pad during all procedures and were given preemptive buprenorphine analgesia (0.1mg/kg) and fluid supplementation (5mL/kg) prior to instrumentation.

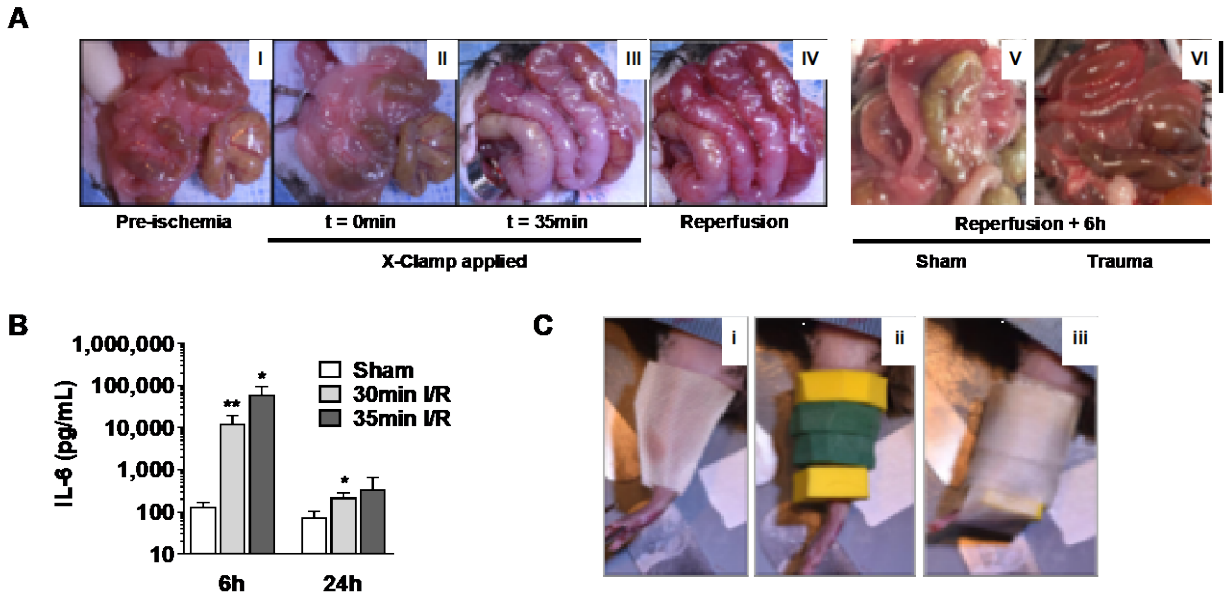

Figure 1. Murine model of polytrauma.
Our polytrauma model included bowel ischemia, bone fracture, and muscle crush to simulate combat injuries, such as those induced by improvised explosion devices. (A) Application of a vascular cross-clamp to the aortic origin of the superior mesenteric artery results in temporary occlusion of blood flow to the bowel (Panel II: X-Clamp t=0, III: X-Clamp t=35min) with restoration of perfusion following removal of the clamp (Panel IV). Compared to normal healthy bowel before (Panel I) and after sham laparotomy (Panel V), grossly edematous and dilated bowel is seen (Panel VI) following SMA I/R. (B) Increasing ischemia time from 30 min to 35 min exacerbates inflammatory responses at 6h and 24h. (C) Alignment and reduction of fractured lower limb by tape splinting (Panel i), and externally fixated using a hollow foam boot cast (Panel ii-iii). The animal in this image is under anesthesia. *P<0.05, **P<0.01 vs. Sham control, Student's t test or nonparametric analysis Mann-Whitney test.

3.3 Blood and solid tissue sample collection

Animals were euthanized at 6 hours (h), 24h, or 14 days (d) following polytrauma or sham procedure by cardiac puncture under general anesthesia. Blood samples were collected in K2EDTA phlebotomy tubes (MiniCollect, Greiner Bio One, Monroe, NC) and immediately processed by two-step centrifugation, at 1,000 grams (g) and 10,000g for 10min at 4°C to obtain a cell-free plasma aliquot, which was stored at -80°C until further analysis. Tissues, thoracic, and abdominal organ samples were collected sterilely and rinsed in cold phosphate buffered saline (PBS). Samples for RNA and protein analyses were immediately snap frozen in liquid nitrogen and stored at -80°C until further analysis.

3.4 Tissue histology

Organs were collected, rinsed in PBS, and immersed in 10% neutral buffered formalin (NBF) for 24h-48h. Uniquely, lung samples were instilled with NBF at 25 centimeters of water (H_2O) or 10min via an intratracheal catheter to maintain alveolar recruitment. Small bowel segments were first flushed with PBS to remove all luminal contents prior to immersion in NBF. All specimens were subsequently embedded in paraffin and 4-micrometer (μm) sections were stained with standard hematoxylin & eosin (H&E).

3.5 Measurement of plasma cytokines and organ injury serum markers

Plasma IL-6 and Tumor necrosis factor-alpha (TNF-α) were tested using enzyme-linked immunosorbent assay (ELISA) kits (R&D Systems, St. Paul, MN). Myoglobin concentration was detected by ELISA (Life Diagnostics, West Chester, PA). ALT and AST activity were determined by colorimetric enzyme activity assay kits (Sigma-Aldrich, St. Louis, MO).

3.6 Mouse echocardiography

Mouse echocardiography was performed using a 13.0 megahertz linear probe (Vivid 7; GE Medical Systems, Chicago, IL) under light anesthesia (ketamine 20mg/kg IP) at 6h and 24h following the surgical procedures. Both B- and M-mode images were obtained with parasternal short axis (SAX) and longitudinal axis (LAX) views. Image analysis was performed offline using Vevo Lab PC software (FUJIFILM VisualSonics, Bothell, WA). left ventricular internal diameter end diastole (LVIDd) and left ventricular internal diameter end systole (LVIDs) were measured from SAX images obtained at the level of the papillary muscles. Stroke volume (SV) was determined by the change in LV cavity area between systole and diastole based on LV tracings of SAX and LAX images using Simpson's biplane method. Cardiac output (CO) and fraction shortening (FS) were calculated as HR x SV, and (LVIDd-LVIDs)/LVIDd, respectively.

3.7 RNA extraction and quantification

RNA was extracted from homogenized tissues or cells using TRIzol reagent according to the manufacturer's protocol (Life Technologies, Waltham, MA). For plasma RNA extraction, TRIzol LS reagent was mixed with 50uL of plasma samples along with 9.9amol of *Caenorhabditis elegans* mir-39 (cel-mir-39) as a spike-in control and processed according to the manufacturer's protocol. To improve RNA recovery yield, 5 micrograms (μg) of glycogen (Invitrogen, Waltham, MA) was added to samples during alcohol precipitation and chilled at -20°C for 18hours. The purified RNA pellet was then resuspended in diethyl pyrocarbonate (DEPC) H_2O for further analysis. Total purified RNA concentration was measured using either a Nanodrop One ultraviolet (UV) spectrophotometer (Thermo Scientific, Waltham, MA) or a fluorometric Quant-it RNA Assay Kit (Life Technologies, Carlsbad, CA). Alternatively, the Bioanalyzer 2100 Small RNA Kit (Agilent Technologies, Santa Clara, CA) was used quantify small RNA.

3.8 Reverse Transcription-quantitative PCR (RT-qPCR)

mRNA gene expression in solid tissues and cells was evaluated as follows. Moloney Murine Leukemia Virus Reverse Transcriptase (M-MLV, Promega, Madison, WI) was used to synthesize complementary DNA (cDNA) from purified template RNA samples. Subsequently, quantitative real-time polymerase chain reaction (qPCR) with GoTaq Master Mix (Promega) was carried out in a QuantStudio 5 PCR thermocycler (Applied Biosystems, Foster City, CA). Relative expression (RE) of mRNA was calculated using the comparative cycle threshold ($2^{-\Delta\Delta CT}$) method normalized to Glyceraldehyde 3-phosphate dehydrogenase (GAPDH) expression.

3.9 miRNA detection

RT-PCR using the miScript SYBR Green PCR kit (Qiagen, Germantown, MD) was performed on cDNA generated from purified RNA samples using the miScript II Reverse Transcriptase kit according to the manufacturer's instructions. Relative expression (RE) was calculated using the $2^{-\Delta\Delta CT}$ method normalized to spike-in cel-miR-39. Sequences for the primers can be found in the supplemental materials.

3.10 RNA sequencing and data analysis

Purified plasma RNA was sequenced by Norgen Biotek (Thorold, ON, Canada) on the Illumina NextSeq500 platform. In brief, small RNA libraries were prepared using the Norgen Biotek Small RNA Library Preparation Kit (Norgen Biotek), and the resultant cDNA was subjected to PCR amplification then purified and size selected by polyacrylamide gel electrophoresis (PAGE) to enrich the miRNA fraction. The library was then analyzed on NextSeq500 sequencer (Illumina, Foster City, CA) with a total of 20M raw reads per sample.

3.11 miRNA differential expression analysis

Adapter sequences and low-quality reads were removed from raw reads using the exceRpt Small RNA-seq Pipeline (Genboree Bioinformatics, Houston, TX). The remaining high-quality reads were aligned to the following reference databases: mouse miRNA (miRbase.org v.21), mouse genome (C57BL/6J:mm9), tRNA (gtRNAdb), and piRNA (RNAdb). miRNAs with a minimum read count of 5 and were used to perform statistical analysis and determine differentially expressed miRNAs in subsequent bioinformatics analysis. Using the edgeR package in the R programming environment, read counts were normalized using the trimmed mean of M-value (TMM) method for differential expression analysis between sham and polytrauma groups with the Benjamini-Hochberg procedure for adjusting the false discovery rate (FDR). Statistically significant differentially expressed miRNAs is defined as a fold change (FC) $\geq$ or ≤ 2 of sham vs. trauma at *p*-value and FDR <0.05. Volcano plot analysis was constructed by plotting $-\log_{10}$(FDR) against $\log_2$FC to identify the most highly statistically significant differentially expressed miRNAs, while the most variably expressed (i.e. largest % Coefficient of variant (CV) of DE) 50 miRNAs were selected for hierarchical cluster analysis.

3.12 Cell culture and reagents

Bone marrow-derived macrophages (BMDMs) were isolated and cultured as follows. Myeloid progenitor cells were isolated from bone marrow flushed from the femurs and tibias of 8- to 12-week old male or female mice and cultured in the presence of macrophage colony-stimulating factor (M-CSF, R&D Systems). Cells were resuspended in RPMI-1640 growth medium supplemented with 10% FBS, 5% horse serum, and penicillin/streptomycin (100U/mL)/(100µg/mL) and seeded at a density of 2M/mL on 6-well, 12-well, 24-well, or 96-well plates (5mL, 2mL, 0.5mL, or 0.1mL/well, respectively) in an incubator at 37°C with 5% carbon dioxide. Growth medium was replaced after 48hr after initial plating, and at 72h BMDMs were approximately 70-80% confluent and ready for experiments.

3.13 miRNA mimics

miRNA mimics were ordered from Integrated DNA Technologies (IDT, Redwood City, CA) as lyophilized single strand RNA (ssRNAs) with phosphorothioate internucleotidic linkages synthesized and purified by high-pressure liquid chromatography (HPLC). ssRNAs were resuspended in sterile Dnase/Rnase-free DEPC-treated H_2O and diluted to working concentrations. A complete list of the miRNAs used in this study and their sequences is included in the supplemental figures.

3.14 Cell treatments

BMDMs were serum starved for 1h prior to cell treatment by replacing growth medium with RPMI-1640 + 0.05% BSA. Synthetic miRNA mimics (various, 0-5000nM) were complexed with Lipofectamine 3000 transfection reagent (1.5 microliters per milliliters (µL/mL); Invitrogen)

and incubated for 5 min at room temperature prior to addition of the RNA-lipid complex to cells. Lipofectamine (1.5µL/mL), poly(I:C) (10µg/mL; Enzo Life Sciences, Farmingdale, NY), R837 (1µg/mL; InvivoGen, San Diego, CA), or Pam3Cys (1 microgram per milliliter (µg/mL); Enzo Life Sciences) were added directly to wells. Culture medium was collected 18h after treatment for analysis by ELISA or Western blot.

3.15 Western blot

Secreted proteins from equal volumes of cell culture medium were separated in a 4-20% gradient Tris-HCl SDS-PAGE, transferred to polyvinylidene difluoride membranes, and immunoblotted overnight at 4°C with goat anti-human cfB antibody (1:2,500 dilution, Complement Technology, Tyler, TX) in tris buffered saline (25 millimolar (mM) Tris-HCl, pH 8.8, 190mM Sodium chloride (NaCl), 0.1% Tween 20) (TBST) + 5% nonfat dry milk. The blot was subsequently probed 24h later with Horseradish peroxidase (HRP)-conjugated rabbit anti-goat IgG secondary antibody (1:10,000 dilution, Sigma-Aldrich) in TBST + 5% nonfat dry milk, then visualized using Luminata Forte Western HRP substrate (Millipore, St. Louis, MO).

3.16 Flow cytometry analysis

To characterize leukocyte population and subpopulations, $5x10^5$ cells were incubated at 4°C for 10 min (light protected) with anti-mouse CD-45, Ly-6G, F4/80, and Ly-6C cell surface marker antibodies directed against murine leukocytes, neutrophils, monocytes, and macrophages. Flow cytometric analysis (20,000 events) was then performed on a LSR II flow cytometer (BD Biosciences, Franklin Lakes, NJ). Data was abstracted using FlowJo (Tree Star, Inc., Ashland, OR) according the depicted gating strategy (not shown).

3.17 Statistical analysis

Continuous variables were expressed as mean +SE [95% confidence interval (CI)] for normally distributed data and median (25^{th}, 75^{th} percentile for non-normal distributions). Categorical data are described or presented as n (%). Results depicted are representative data obtained in two to three independent experiments using a minimum of animals per endpoint; all results are presented. Statistical comparisons between groups were performed by Analysis of Variance (ANOVA), while Student's *t* test or Mann-Whitney *U*-test was used for paired continuous data, and the Mantel-Cox test was used for survival curve analysis. Analyses were performed using GraphPad Prism 6 (GraphPad, San Diego, CA). A p value <0.05 was considered statistically significant.

4.0 RESULTS AND DISCUSSIONS

4.1 Part I: Trauma, miRNA, and inflammation

4.1.1 Polytrauma induces marked local and systemic inflammation and multiple organ injury

We established a murine polytrauma model with the three components (bowel ischemia, bone fracture, and muscle crush) that represent the type of injury often occurred after improvised explosion. Once established, we systematically examined inflammation and local and remote organ injury. Polytrauma mice initially exhibited clinical signs of circulatory shock with lower core temperature at 2- and 6- hours after the procedure but recovered at 24 hours (**Fig. 2A**). As expected, the polytrauma resulted in severe bowel and skeletal muscle injury as evidenced by widespread intestine mucosal damage, including severe villous blunting, marked neutrophil infiltration, and patchy mural necrosis with sloughing of the mucosa (**Fig. 2B**). Tibial fracture and muscle crush resulted in muscle interstitial edema and necrosis (**Fig. 2C**), marked increases in muscle tissue inflammatory cytokine genes (such as IL-1β, IL-6, and TNF-α)(**Fig. 2D**), and a rise in plasma myoglobin at 6 hours post-injury (**Fig. 2E**).

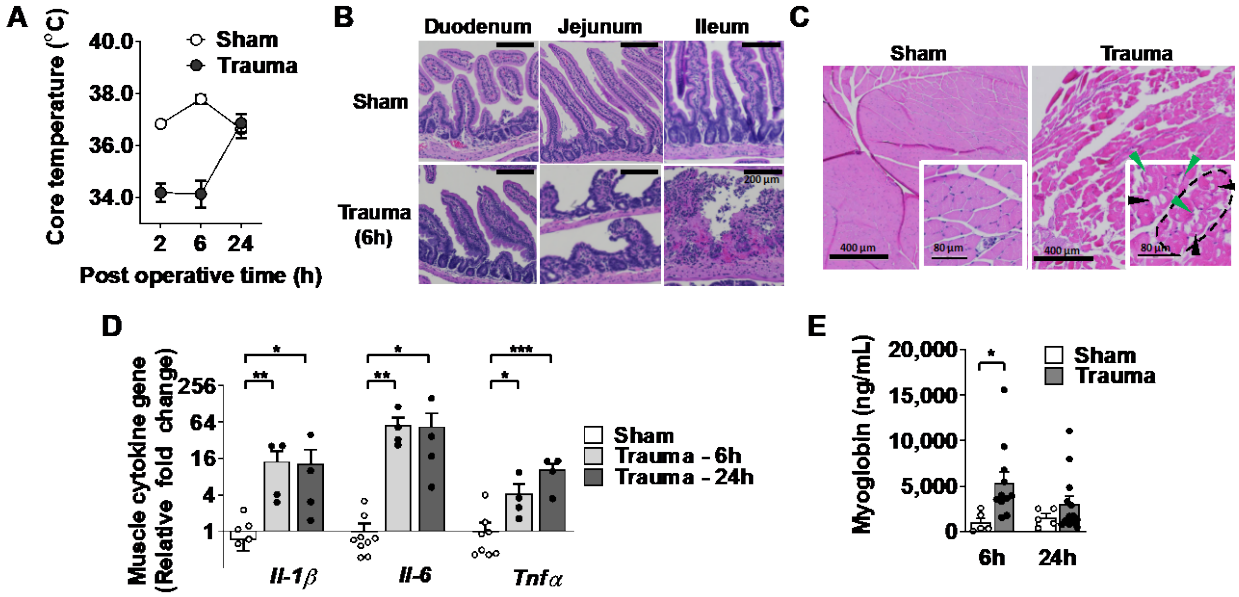

Figure 2. Polytrauma induces circulatory shock and tissue injury in bowel and muscle.
(A) Polytrauma causes significant systemic shock, as manifested by reduced core body temperature at 2- and 6-h post injury versus sham mice. (B) H&E staining shows injury throughout the small bowel ranging from inflammatory cell infiltration, separation of the epithelium and the luminal basal layers, villous blunting, and near-complete disintegration of epithelial layers; sham mice display no observable mucosal damage. (C) H&E staining shows that muscle crush injury results in loss of organized muscle fascicle architecture (dotted line), severe intracellular vacuolization (black arrows), and global disruptions in muscle fibre cell membrane (green arrows). (D) A significant increase in muscle tissue inflammatory cytokine genes is observed at 6- and 24-h post-injury. Data are normalized to control GAPDH expression and compared with sham. (E) Plasma myoglobin levels are elevated at 6-h as a consequence of traumatic rhabdomyolysis. *P<0.05, **P<0.01, ***P<0.001, ****P<0.0001, Student's t test or nonparametric analysis Mann-Whitney test.

Polytrauma also led to a marked increase in plasma IL-6 and TNF-α levels at both 6- and 24-h following trauma (**Fig. 3A**) and resulted in multiple instances of remote organ dysfunction and injury. As measured by echocardiography, there was a significant decrease in SV and CO 6 hours after polytrauma, with subsequent return of cardiac function to within normal limits by 24 hours (**Fig. 3B**). We also observed acute kidney injury (AKI) at 6 and 24 hours post-injury, as demonstrated by marked increases in the gene expression of AKI biomarkers (kidney injury molecule-1 (KIM-1) and Neutrophil gelatinase-associated lipocalin (NGAL)) in the kidney, increases in plasma creatinine, and acute tubular necrosis (**Fig. 3C-D**); additionally, we observed acute hepatic injury, as evidenced by increased AST and bile duct proliferation on histology (**Fig. 3E**).

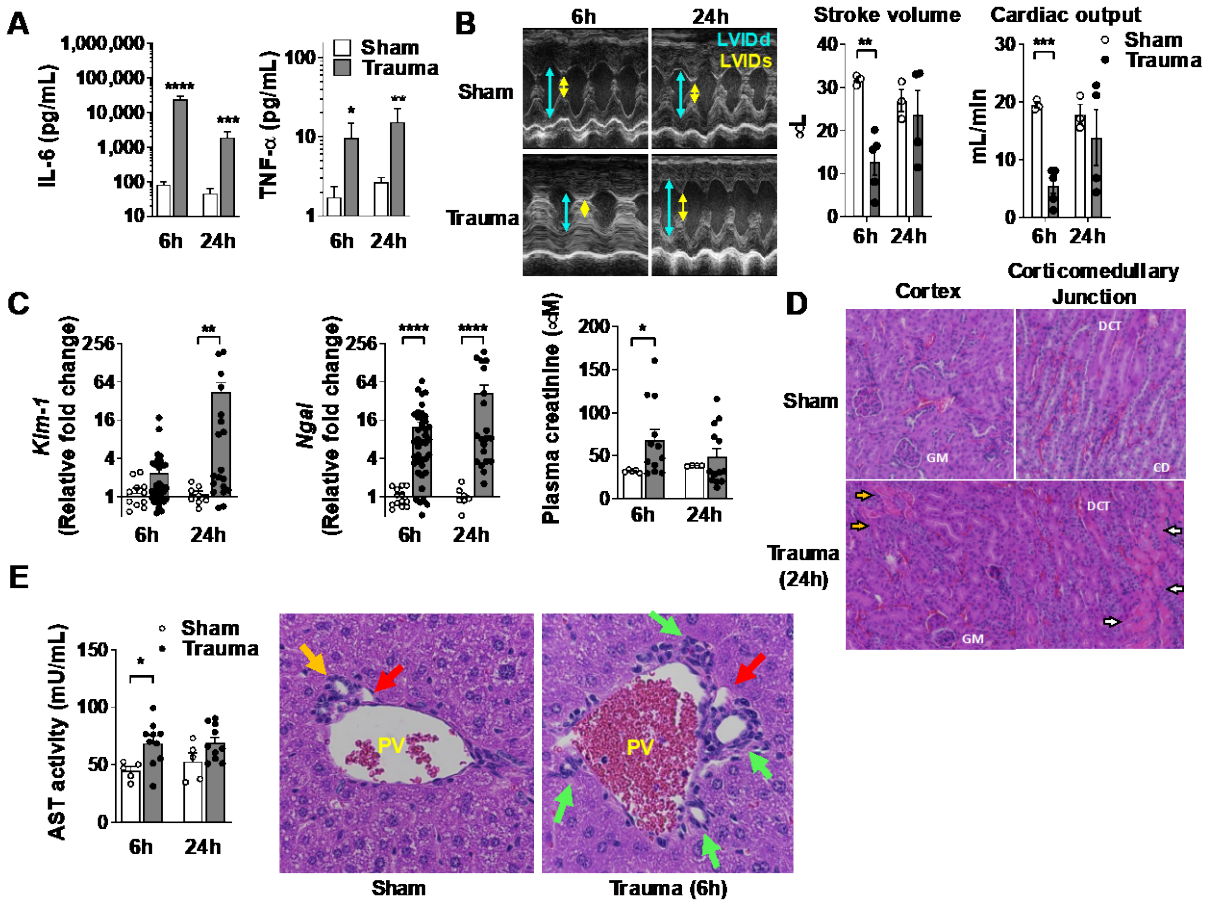

Figure 3. Polytrauma induces systemic inflammation and remote multiorgan injury.
(A) Polytrauma resulted in increased plasma levels of IL-6 and TNF-α at 6- and 24- hours post injury. (B) Echocardiography (echo) of sham or polytrauma mice at 6- and 24-hours post injury. Stroke volume and cardiac output were evaluated via analysis of the echo. (C) Elevations of gene expression (KIM-1 and NGAL) and plasma creatinine levels at 6- and 24-hours post-polytrauma. (D) H&E staining of the kidney shows acute tubular necrosis at 24-hours post-injury versus sham (arrows). (E) Elevated AST was observed in polytrauma mice (6- and 24-hr post-injury). H&E staining of kidneys from sham or polytrauma mice (6h post-injury) shows bile duct proliferation in polytrauma tissues (green arrows).

4.1.2 Polytrauma leads to marked increase in plasma RNA and many miRNAs n

Using high-resolution automated electrophoresis (Bioanalyzer 2100, Agilent, Santa Clara, CA) (**Fig. 4A**), we observed a significant rise in the expression of a group of small RNAs between 10-150 nucleotides in size (112±27 vs. 399±45 nanograms per milliliter (ng/mL, $p<0.001$) in the plasma at 6 hours post-polytrauma injury compared with sham (**Fig. 4B**). The plasma small RNA concentrations returned to baseline at 24 hours post-injury. Interestingly, plasma small RNA concentrations highly correlated with the plasma IL-6 expression and kidney NGAL expression (RNA vs IL-6, $R=0.75$, $p<0.0001$, RNA vs NGAL, $R=0.58$, $p<0.01$). To define the type of plasma RNAs and quantify the change of miRNAs following traumatic injury, we performed plasma RNAseq analysis. Out of total reads (166,357,230) assigned to the 15 samples and mapped to the mouse genome, 92.7% were miRNAs, 8.4% rRNA, 2.0% mRNA, % piRNA, and 0.9% tRNA (**Fig. 4C**). Interestingly, unmatched RNAs, including small bacterial RNAs, constituted only 4.0% of all plasma small RNAs. As illustrated in **Fig. 4D-E**, the Volcano plot and heatmap clearly indicated a distinct miRNA expression pattern between sham and polytrauma mice and identified 80 up- and 62 down-regulated miRNAs (data not shown). This part of data will be further analyzed using bioinformatics.

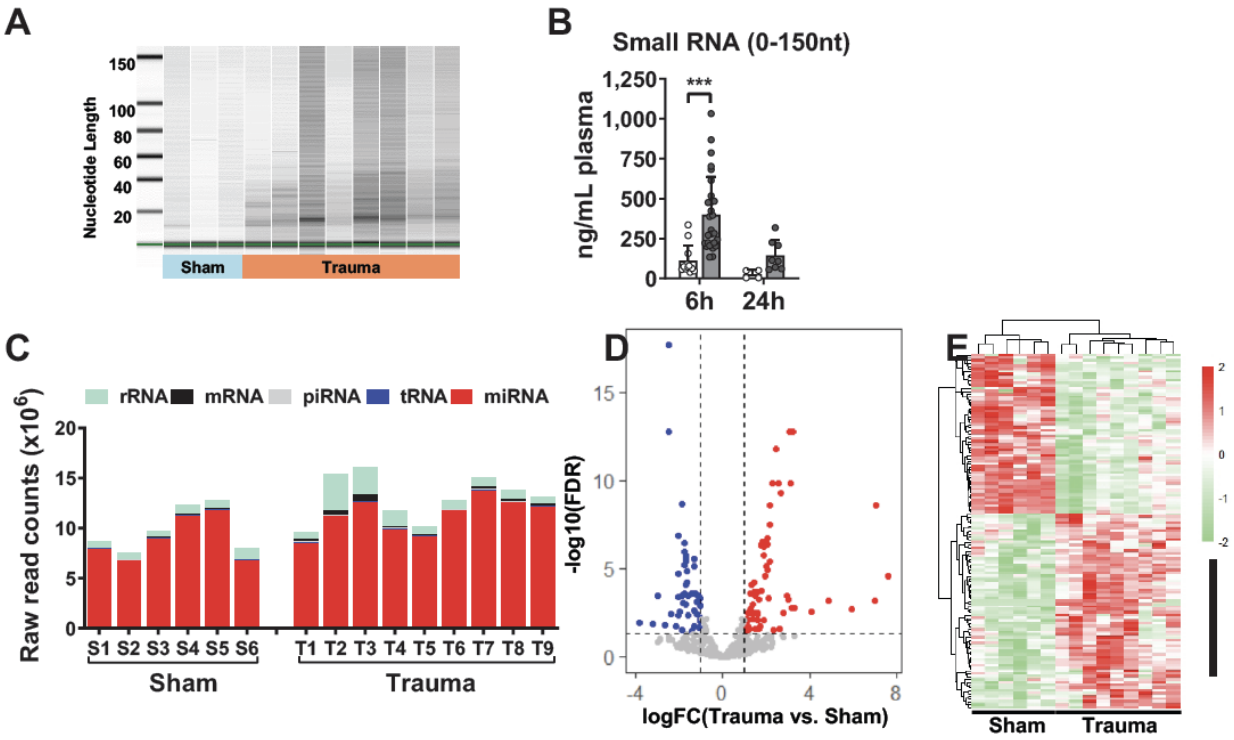

Figure 4. Polytrauma increases plasma RNA and alters plasma miRNA profile
(A) High-resolution automated electrophoresis of RNA isolated from sham or polytrauma mice at 6-hr post-injury (B) Quantification of small RNA (0-150nt) levels (identified in panel A) in the plasma of mice at 6- or 24-hours post-injury in polytrauma versus sham mice. (C) Raw read counts of various RNA subtypes from RNA-seq analysis of plasma from sham or polytrauma mice at 6-hr post-injury. Volcano plot (D) and heatmap (E) of miRNA expression patterns in sham and polytrauma mice at 6-hr post-injury.

4.1.3 Extracellular RNA and miRNA mimics trigger specific proinflammatory responses in macrophages

In order to assess the ability of the circulating RNA found in polytrauma to induce inflammatory responses, BMDMs were treated with endogenous plasma RNA isolated from sham or polytrauma mice. We observed that effective doses of 0.25µg/mL of plasma RNA from polytrauma mice induced robust IL-6 and Chemokine CXC ligand-2 (CXCL-2) (a.k.a. MIP-2) production in macrophages, whereas equivalent amounts of plasma RNA from sham mice did not, suggesting that RNA that are released into plasma are intrinsically pro-inflammatory (**Fig. 5A**). Given the predominant biotype of plasma RNA is miRNA, we examined the innate immune activity of plasma miRNAs following trauma. Eighteen miRNAs identified by RNAseq to be upregulated (>2-fold), abundant (based on read counts), and highly statistically significant (FDR and *p*-value <0.05), and with various abundance of uridines (U) in their sequences as stratified as low (<20% U), moderate (≥20 to <40% U), and high (≥40 % U), respectively (**Table 1**), were selected and tested for an immunostimulatory response in macrophages. Among the 18 miRNAs tested, nine (let-7b, -7j, -7a, miR-34a, -122, -142a, -145a, -146a, -802) induced a dose-dependent production of MIP-2 and IL-6 (**Fig. 5C**), each with an EC_{50} at sub-µM, whereas the other nine failed to induce cytokine production (data not shown). Further analysis of nucleotide compositions of these miRNAs clearly indicates that those pro-inflammatory miRNA mimics tended to have higher U abundance compared to those of non-inflammatory while such association was absence with adenosine (A), cytidine (C), or guanosine (B) (**Fig. 5B**).

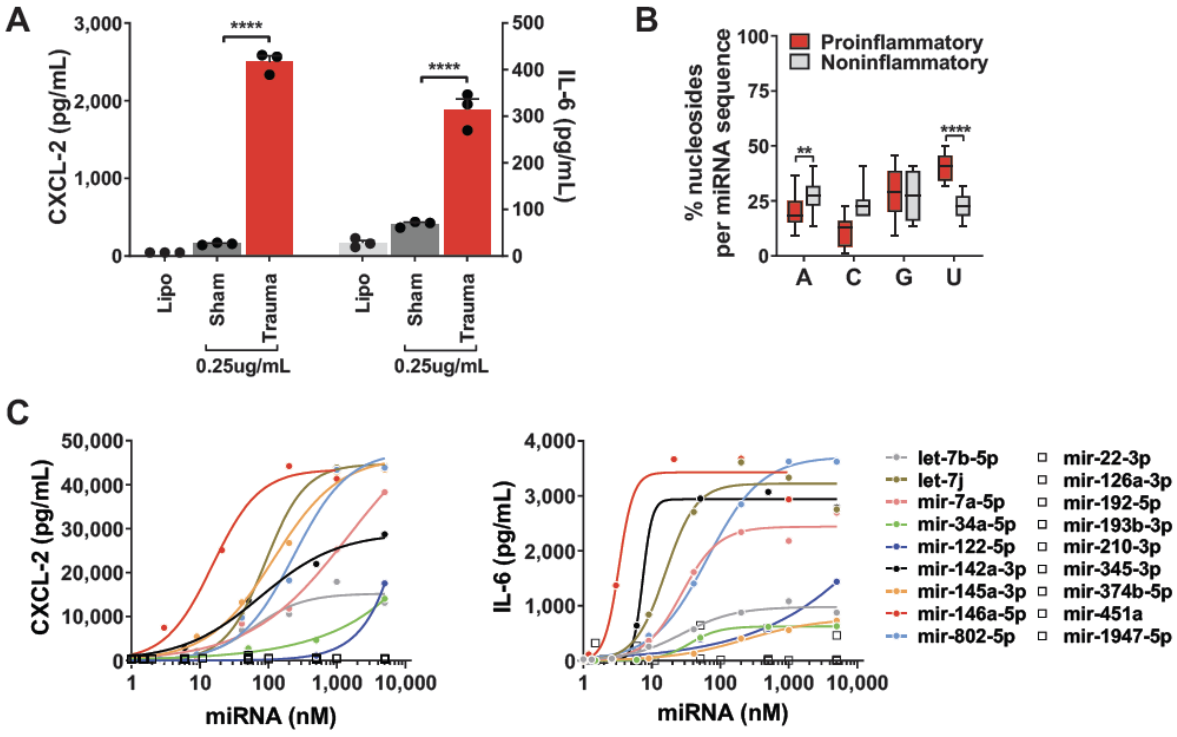

Figure 5. RNA and miRNA mimics trigger macrophage proinflammatory responses
(A) Treatment of BMDMs with plasma RNA isolated from polytrauma mice induced increased levels of the pro-inflammatory markers CXCL-2 and IL-6 compared to sham. (B) Analysis of the nucleotide composition of miRNAs identified as proinflammatory (red) versus noninflammatory (gray). (C) Analysis of the eighteen miRNAs identified as upregulated by RNAseq tested in macrophages to determine the immunostimulatory response in BMDMs, as evidenced by their ability to induce CXCL-2 or IL-6 production.

Table 1. List of miRNAs used in the study.
Single-stranded miRNA mimics used in this study, rank list ordered by U residuce content in each miRNA (%U = #U / # of total nucleotides in miRNA x 100%).

miRNA	Sequence (5' - 3')	Length (nt)	Uridine # (%)	Stratify by %U
let-7j	UGAGGUAUUAGUUUGUGCUGUUAU	24	12 (50)	High (≥40)
mir-142a-3p	UGUAGUGUUUCCUACUUUAUGGA	23	11 (48)	
mir-7a-5p	UGGAAGACUAGUGAUUUUGUUGU	23	10 (43)	
let-7b	UGAGGUAGUAGGUUGUGUGGUU	22	9 (41)	
mir-34a-5p	UGGCAGUGUCUUAGCUGGUUGU	22	9 (41)	
mir-145a-3p	AUUCCUGGAAAUACUGUUCUUG	22	9 (41)	
mir-122-5p	UGGAGUGUGACAAUGGUGUUUG	22	8 (36)	Moderate (≥20 to <40)
mir-146a-5p	UGAGAACUGAAUUCCAUGGGUU	22	7 (32)	
mir-802-5p	UCAGUAACAAAGAUUCAUCCUU	22	7 (32)	
mir-451a	AAACCGUUACCAUUACUGAGUU	22	7 (32)	
mir-126a-3p	UCGUACCGUGAGUAAUAAUGCG	22	6 (27)	
mir-374b-5p	AUAUAAUACAACCUGCUAAGUG	22	6 (27)	
mir-192-5p	CUGACCUAUGAAUUGACAGCC	21	5 (24)	
mir-22-3p	AAGCUGCCAGUUGAAGAACUGU	22	5 (23)	
mir-210-3p	CUGUGCGUGUGACAGCGGCUGA	22	5 (23)	
mir-345-3p	CCUGAACUAGGGGUCUGGAGAC	22	4 (18)	Low (<20)
mir-1947-5p	AGGACGAGCUAGCUGAGUGCUG	22	4 (18)	
mir-193b-3p	AACUGGCCCACAAAGUCCCGCU	22	3 (14)	

4.1.4 Identification of TLR7-mediated induction of immune inflammatory responses by uridine-rich miRNAs

Given the critical role of U moieties in the activation of TLR7 by single-stranded RNA[14], we subsequently assessed the inflammatory properties of circulating miRNAs in polytrauma based on their U content (%U). Compared to the non-inflammatory ex-miRNAs identified in **Fig. 5C**, we observed that miRNAs capable of inducing cytokine responses were more likely to contain more U (pro- vs non-inflammatory, 40±2% vs 23±2%, $p<0.0001$). Moreover, in separate experiments with different endpoints, we found that miRNAs with high %U (>40%), such as let-7j, miR-145a-3p, miR-7a-5p, all induced cytokine and complement factor B (FB) production, whereas those with low %U (<20%), such as miR-1947-5p, miR-345-3p, miR-193b-3p, failed to do so (**Fig. 6A-B**). Thus, these findings further confirm that miRNAs containing high U abundance exhibit greater immunostimulatory potential than those with lower U contents and indicate that the presence of U nucleobases is a key element in the immune recognition of miRNAs.

Finally, we conducted a series of loss-of-function experiments to determine the necessity of TLR3 or TLR7 in mediating FB and cytokine production in cells treated with miRNA mimics or various TLR agonists. As indicated in **Fig. 6C**, FB and cytokine (data not shown) responses to various miRNA mimics and the TLR7 agonist R837 were completely abolished in TLR7$^{-/-}$ cells but retained in TLR3$^{-/-}$ cells. Of note, FB and MIP2 (not shown) production was attenuated in TLR3$^{-/-}$ cells when stimulated by Poly(I:C) (TLR3 agonist) but not Pam3cys. These data suggest that the miRNA-induced innate immune activation, as measured by cytokine and FB production, is entirely TLR7-dependent.

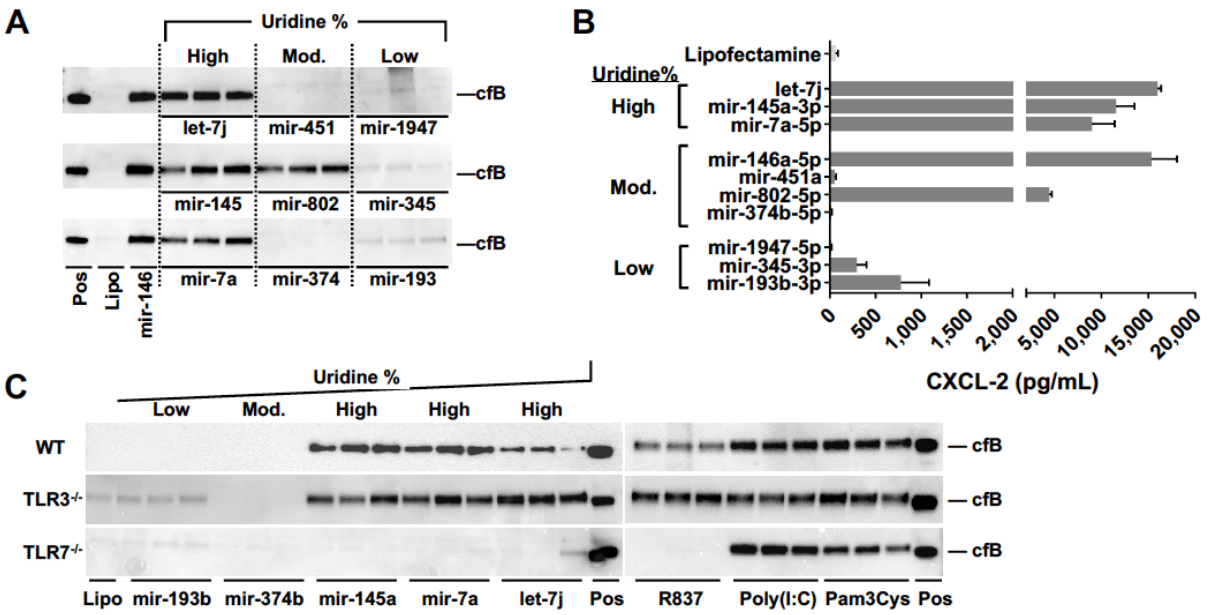

Figure 6. Role of U content in miRNA-induced FB production in macrophages.
(A) Western blot analysis of complement factor B expression following treatment of BMDMs with miRNAs containing high, moderate, or low U content. (B) Analysis proinflammatory CXCL-2 levels in BMDMs following treatment with miRNAs containing high, moderate, or low U content. (C) Western blot analysis of complement factor B expression after treatment of BMDMs from wild type (WT), TLR3, or TLR7 knockout mice (TLR3-/- and TLR7-/-, respectively) with miRNAs containing high, moderate, or low U content.

4.2 Part II. Impact of hypobaria on organ injury after trauma[15]

4.2.1 Polytrauma induces severe bradycardia, hypothermia, and cytokine storm

Fig. 7A illustrates the experimental flow of this set of studies. Two hours after the trauma or sham procedure, mice were randomized to undergo six hours of either normoxic/normobaric or normoxic/hypobaric conditions (**Fig. 7**). At 8 hours post-injury (at the end of the treatments), mice underwent echocardiography. For some mice, echocardiography was performed again at 24 hours. At either 8- or 24-hours, mice were anesthetized with intraperitoneal ketamine (100 mg/kg) and xylazine (4 mg/kg). Following confirmation of general anesthesia, bronchoalveolar lavage (BAL) was performed, whole blood was collected by cardiac puncture, and kidneys were collected and snap-frozen in liquid nitrogen. Processed plasma, BAL fluid, and kidneys were stored at -80 °C until assays were performed. Heart rate was measured in all groups under normobaric conditions at baseline, then again at 8- or 24-hours after surgical procedures by echocardiography. As shown in **Fig. 7B**, compared with sham mice, polytrauma mice developed significant bradycardia (665 ± 36 vs. 566 ± 73 beats/min, $p<0.01$) at 8 hours post-injury, and this difference resolved at 24 hours post-injury in surviving mice. Core temperature, reflecting circulatory function, dropped significantly at 8 hours post-injury as compared with sham (35.5 ± 0.7 vs. 32.9 ± 2.4 °C, $p<0.01$), but returned to normal at 24 hours post-injury (**Fig. 7C**). At 8 hours post-injury, polytrauma mice exhibited significantly higher levels of plasma IL-6 than sham mice (57 ± 14 vs. 1216 ± 2655 picograms per milliliter (pg/mL), $p<0.01$) (**Fig. 7D**), indicating a rapid and robust systemic innate immune response, but returned to the control level at 24 hours post-injury. To assess the impact of hypobaric exposure on polytrauma-induced physiological responses, sham and polytrauma mice were randomized 2 hours after surgical procedures to undergo six hours of either hypobaric or normobaric conditions. Animals were examined either immediately after the simulated 'flight' (8 hours post-injury), or 16 hours after the 'flight' (24 hours post-injury). We found that compared with the normobaric group, the mice exposed to hypobaria exhibited similar degrees of bradycardia, hypothermia, and plasma IL-6 at both 8 and 24 hours (**Fig. 7B-C**).

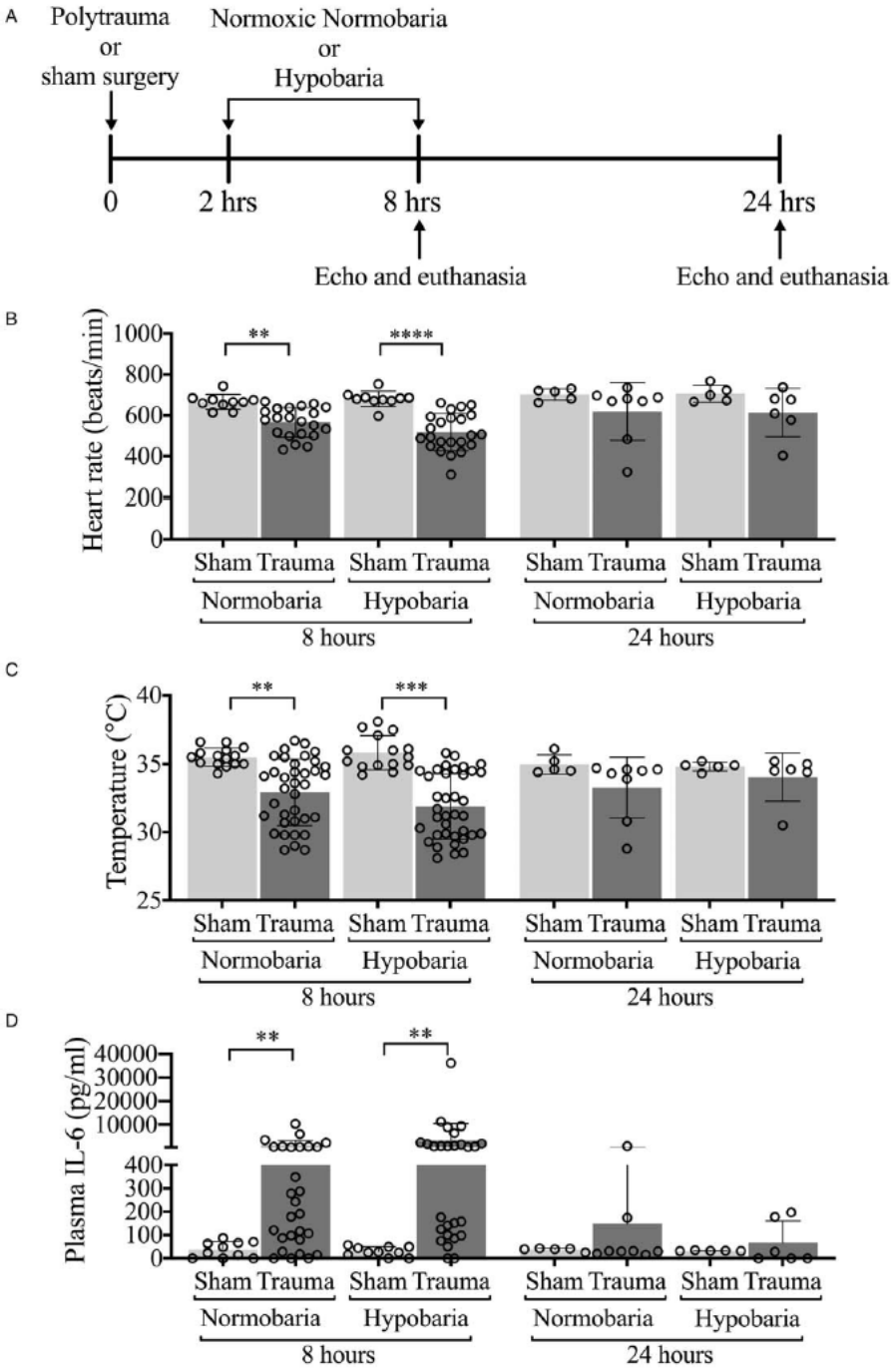

Figure 7. Bradycardia, hypothermia, and cytokine storm in non-hemorrhagic polytrauma.
(A) Timeline/flow chart for the experimental design. Heart rate (B), core temperature (C), or plasma IL-6 levels (D) were measured in sham or trauma mice, exposed to normoxic or hyberbaric conditions for 8- or 24- hours.

4.2.2 Hypobaric exposure exacerbates polytrauma-induced cardiac dysfunction

Cardiac dysfunction has been reported in a subset of trauma patients after injury[16]. We assessed cardiac function via echocardiography at 8- and 24-hours post-injury in all experimental groups. As illustrated in the M-mode images of **Fig. 8** and **Table 2**, 8 hours post-procedure, polytrauma induced a significant decrease in CO as compared with sham group (18.0 ± 2.6 vs. 11.9 ± 5.6 mL/min, $p<0.01$), SV (27.2 ± 4.4 vs. 20.2 ± 8.1 μl/beat, $p<0.05$), LVIDd (2.93 ± 0.17

vs. 2.56 ± 0.38 mm, p<0.05), and LVIDs (1.47 ± 0.16 vs.1.29 ± 0.13 mm, p=0.051). At 24 hours post-injury, polytrauma mice had improved, but still showed a modest decrease in LVIDs (1.53 ± 0.05 vs. 1.40 ± 0.07 mm, p<0.05). There were no significant differences in ejection fraction or fractional shortening between polytrauma and sham at either time point. After exposure to hypobaria, polytrauma mice had significantly decreased ejection fraction (81.0 ± 7.4 vs. 74.2 ± 8.9 %, p<0.01) and fractional shortening (48.5 ± 7.9 vs. 41.8 ± 8.1%, p<0.01) at 8 hours post-injury. These differences resolved at 24 hours post-injury. Notably, there was no significant difference in CO, SV, LVIDd, or LVIDs between polytrauma mice exposed to hypobaria and those kept at normobaria at either time point.

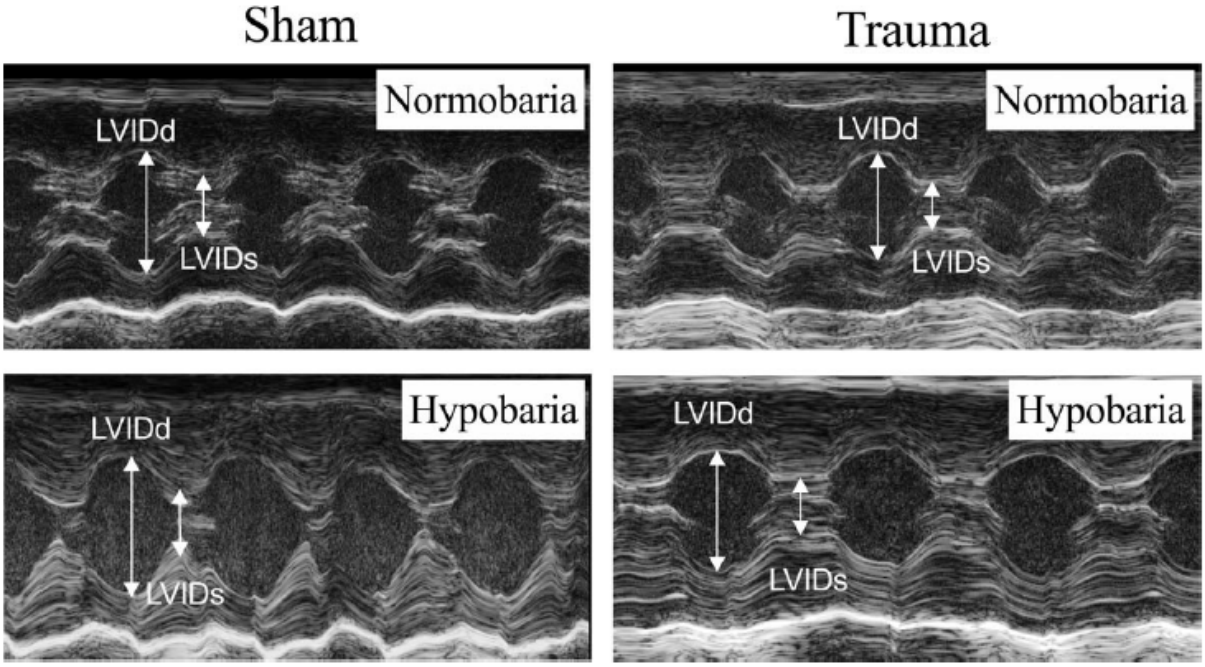

Figure 8. Representative echocardiographic M-mode images at 8hr post-injury.
Images were collected for sham and polytrauma mice, exposed to normobaria or hypobaria at 8hr post-injury. LVIDd, end-diastolic left ventricular internal dimension; LVIDs, end-systolic left ventricular internal dimension.

Table 2. Impact of hypobaria on echocardiography parameters at 8- and 24-h post-injury

	Sham Normobaria		Polytrauma Normobaria		Sham Hypobaria		Polytrauma Hypobaria	
	Mean	***SD***	***Mean***	***SD***	***Mean***	***SD***	***Mean***	***SD***
8 hours post-injury								
Cardiac output (ml/min)	18.02	2.64	11.91^{**}	5.61	18.45	2.03	$8.72^{\Delta\Delta\Delta\Delta}$	5.14
Stroke volume (∝l/beat)	27.19	4.45	20.24^{*}	8.14	27.13	2.65	$16.48^{\Delta\Delta\Delta}$	9.14
Ejection fraction (%)	82.50	4.53	81.03	7.37	83.19	3.71	$74.16^{\Delta\Delta,\ddagger\ddagger}$	8.86
Fractional shortening (%)	50.04	5.12	48.54		50.68	4.12	$41.77^{\Delta\Delta,\ddagger\ddagger}$	8.11
LVIDd (mm)	2.931	0.170	2.558^{*}	0.375	2.907	0.145	$2.419^{\Delta\Delta}$	0.461
LVIDs (mm)	1.466	0.165	$1.292^{\#}$	0.134	1.448	0.182	1.395	0.261
24 hours post-injury								
Cardiac output (ml/min)	19.22	3.93	14.39	5.78	17.07	3.74	14.37	5.40
Stroke volume (∝l/beat)	27.26	4.62	22.40	6.56	24.20	5.37	22.64	5.47
Ejection fraction (%)	80.89	1.87	80.35	5.50	79.35	4.40	83.54	3.06
Fractional shortening (%)	48.05	2.10	47.55	5.64	46.54	4.47	50.73	3.68
LVIDd (mm)	2.954	0.172	2.695	0.316	2.828	0.195	2.668	0.259
LVIDs (mm)	1.534	0.048	1.401^{*}	0.089	1.488	0.088	1.345^{Δ}	0.061

Echocardiography parameters at 8 and 24 hours post-injury. LVIDd, end-diastolic left ventricular internal dimension; LVIDs, end-systolic left ventricular internal dimension. #p=0.051, *p<0.05, **p<0.01 compared to sham-NB; Δ p<0.05, ΔΔ p<0.01, ΔΔΔ p<0.001, ΔΔΔΔ p<0.0001 compared to sham-HB; ‡‡ p<0.01 compared to polytrauma-NB. NB, normobaria; HB, hypobaria. n=5-23/group. Data was analyzed by Two-way ANOVA with Bonferroni's post hoc test.

4.2.3 Hypobaric exposure worsens endothelial injury in polytrauma

We assessed the impact of polytrauma on endothelial cell activation and glycocalyx integrity by measuring plasma concentrations of several endothelium-associated molecules. A healthy endothelial glycocalyx has numerous components, including proteoglycans and glycoproteins that bind to negatively charged side chains called glycosaminoglycans (**Fig. 9A**). To detect glycocalyx degradation, we measured soluble hyaluronic acid, a glycosaminoglycan; syndecan-1, a proteoglycan; and thrombomodulin, a glycoprotein. To assess endothelial activation, we measured soluble E-selectin, an inducible glycoprotein expressed on the vascular endothelium after injury. As shown in **Fig. 9B**, polytrauma led to significantly elevated plasma concentrations of hyaluronic acid (96 ± 38 vs.199 ± 80 ng/mL, p<0.01), thrombomodulin (23.2 ± 3.0 vs. 58.9 ± 22.3 ng/mL, p<0.001), syndecan-1 (0.99 ± 1.29 ng/mL vs. 4.34 ± 3.22 ng/mL, p<0.05), and E-selectin (38.6 ± 10.9 vs. 62.7 ± 24.3 ng/mL, p<0.01) at 8 hours post-trauma; at 24 hours, hyaluronic acid (64.9 ± 28 vs. 360 ± 412 ng/mL), thrombomodulin (29.1 ± 3.1 vs. 37.8 ± 10.1 ng/mL), and E-selectin (34.6 ± 8.3 vs. 56.7 ± 24.9 ng/mL) trended elevated without statistical significance. Trauma mice exposed to hypobaria had significantly higher levels of glycocalyx degradation than trauma mice under normobaric conditions, as indicated by higher plasma concentrations of hyaluronic acid (199 ± 80 vs. 260 ± 111 ng/mL, p<0.05), thrombomodulin (58.9 ± 22.3 vs. 75.4 ± 33.9 ng/mL, p<0.05), and syndecan-1 (4.34 ± 3.22 vs. 8.33 ± 4,73 ng/mL, p<0.001) at 8 hours post-injury (**Fig. 9B**). The plasma concentration of E-selectin was not significantly different between trauma mice exposed to hypobaric and those kept at normobaric conditions (**Fig. 9B**).

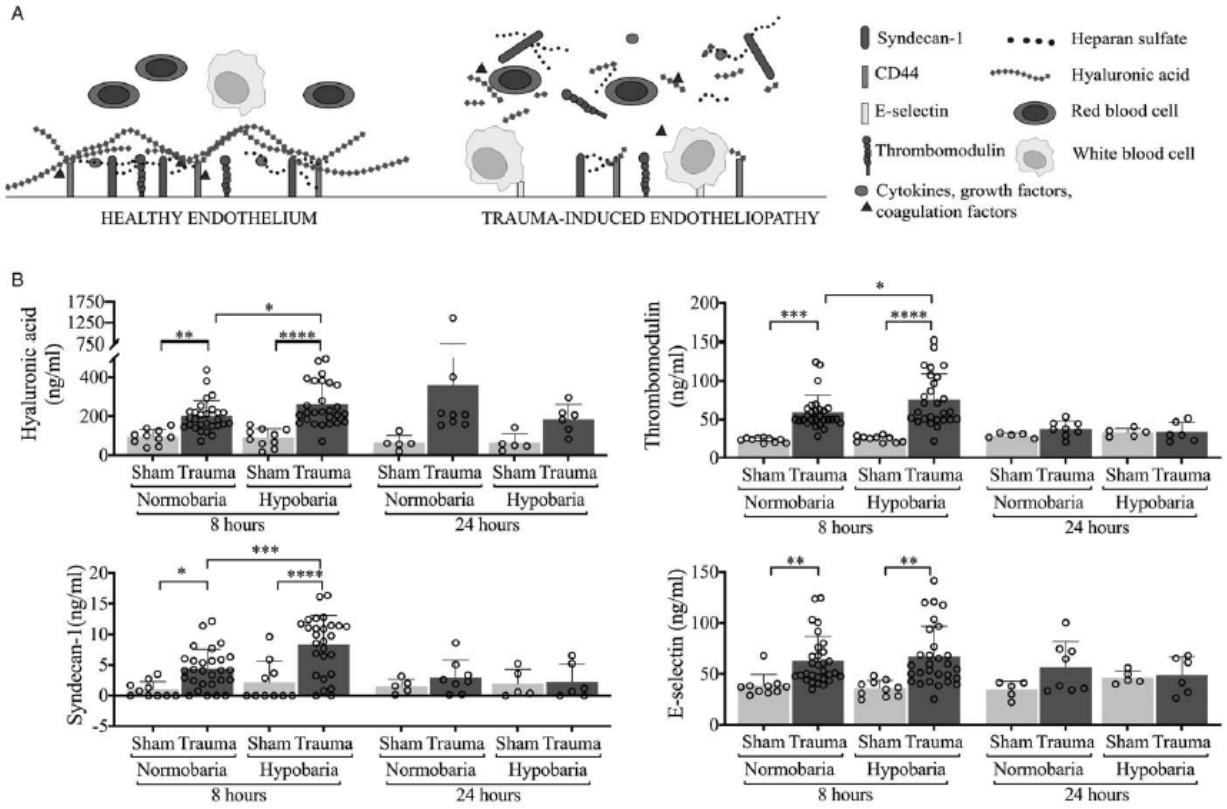

Figure 9. Polytrauma induces endothelial injury.
At 2 hours post-procedure, mice were exposed to normobaric or hypobaric (8000 ft) conditions for 6 hours. (A) Illustration of intact glycocalyx in healthy endothelium and degraded glycocalyx in trauma-induced endothelial injury. At 8- or 24- hours post procedure, mice were euthanized and blood collected by cardiac puncture. (B) Plasma markers of endothelial injury were analyzed by ELISA. SH, Sham; PT, Polytrauma. *p<0.05, **p<0.01, ***P<0.001, ****p<0.0001.

5.0 SUMMARY AND CONCLUSIONS

We have established a combat-relevant polytrauma model that simulates the clinical presentations of injured warfighters. This model is characterized by marked systemic/local inflammation and multiple organ injury including a) local muscle, bone, and bowel injury and b) remote organs - the heart, liver, kidney, and vascular endotheliopathy. The present and future analyses of this model will provide critical information on warfighter injuries that can improve patient care for wounded airmen.

Our results showed that plasma RNA from polytrauma animals is highly proinflammatory. These data support the concept that extracellular RNA, released from tissues upon polytrauma, plays an important role in driving and amplifying systemic inflammation and potentially in inflammatory injury to the organs.

Furthermore, RNA sequencing analysis revealed a large number of single-stranded miRNAs released from tissues following polytrauma. These plasma miRNAs may function as an important driver in inflammatory storm and organ injury often seen post traumatic injury. Certain miRNAs, specifically those with high U abundance, tended to be proinflammatory and induced robust cytokine and complement production via TLR7-mediated mechanisms. These studies shed light into the molecular mechanisms responsible for the immune-stimulatory function of extracellular miRNAs.

Endotheliopathy is a hallmark of inflammation and contributes to organ injury following trauma. In the present study, we demonstrated that hypobaria exposure worsened endothelial injury and cardiac contractile dysfunction in murine polytrauma. This finding suggests a potential “second hit” following initial traumatic injury. Importantly, these data suggest that during AE, high-altitude hypobaric exposure even with adequate oxygen supply may impose harmful effects after traumatic injury.

6.0 REFERENCES

1. Turchinovich A, Tonevitsky AG and Burwinkel B. Extracellular miRNA: A Collision of Two Paradigms. *Trends Biochem Sci*. 2016;41:883-892.

2. Fabbri M, Paone A, Calore F, Galli R, Gaudio E, Santhanam R, Lovat F, Fadda P, Mao C, Nuovo GJ, Zanesi N, Crawford M, Ozer GH, Wernicke D, Alder H, Caligiuri MA, Nana-Sinkam P, Perrotti D and Croce CM. MicroRNAs bind to Toll-like receptors to induce prometastatic inflammatory response. *Proc National Acad Sci*. 2012;109:E2110-6.

3. Lehmann SM, Kruger C, Park B, Derkow K, Rosenberger K, Baumgart J, Trimbuch T, Eom G, Hinz M, Kaul D, Habbel P, Kalin R, Franzoni E, Rybak A, Nguyen D, Veh R, Ninnemann O, Peters O, Nitsch R, Heppner FL, Golenbock D, Schott E, Ploegh HL, Wulczyn FG and Lehnardt S. An unconventional role for miRNA: let-7 activates Toll-like receptor 7 and causes neurodegeneration. *Nat Neurosci*. 2012;15:827-35.

4. Park CK, Xu ZZ, Berta T, Han Q, Chen G, Liu XJ and Ji RR. Extracellular microRNAs activate nociceptor neurons to elicit pain via TLR7 and TRPA1. *Neuron*. 2014;82:47-54.

5. Wang S, Yang Y, Suen A, Zhu J, Williams B, Hu J, Chen F, Kozar R, Shen S, Li Z, Jeyaram A, Jay SM, Zou L and Chao W. Role of extracellular microRNA-146a-5p in host innate immunity and bacterial sepsis. *iScience*. 2021;24:103441.

6. Chen C, Feng Y, Zou L, Wang L, Chen HH, Cai JY, Xu JM, Sosnovik DE and Chao W. Role of extracellular RNA and TLR3-Trif signaling in myocardial ischemia-reperfusion injury. *J Am Heart Assoc*. 2014;3:e000683.

7. Feng Y, Chen H, Cai J, Zou L, Yan D, Xu G, Li D and Chao W. Cardiac RNA induces inflammatory responses in cardiomyocytes and immune cells via Toll-like receptor 7 signaling. *J Biol Chem*. 2015;290:26688-98.

8. Zou L, Feng Y, Xu G, Jian W and Chao W. Splenic RNA and MicroRNA Mimics Promote Complement Factor B Production and Alternative Pathway Activation via Innate Immune Signaling. *J Immunol*. 2016;196:2788-98.

9. Feng Y, Zou L, Yan D, Chen H, Xu G, Jian W, Cui P and Chao W. Extracellular MicroRNAs Induce Potent Innate Immune Responses via TLR7/MyD88-Dependent Mechanisms. *J Immunol*. 2017;199:2106-2117.

10. Zou L, He J, Gu L, Shahror RA, Li Y, Cao T, Wang S, Zhu J, Huang H, Chen F, Fan X, Wu J and Chao W. Brain innate immune response via miRNA-TLR7 sensing in polymicrobial sepsis. *Brain Behav Immun*. 2022;100:10-24.

11. Huang H, Zhu J, Gu L, Hu J, Feng X, Huang W, Wang S, Yang Y, Cui P, Lin SH, Suen A, Shimada BK, Williams B, Kane MA, Ke Y, Zhang CO, Birukova AA, Birukov KG, Chao W and Zou L. TLR7 Mediates Acute Respiratory Distress Syndrome in Sepsis by Sensing Extracellular miR-146a. *Am J Respir Cell Mol Biol*. 2022.

12. Williams B, Zhu J, Zou L and Chao W. Innate immune TLR7 signaling mediates platelet activation and platelet-leukocyte aggregate formation in murine bacterial sepsis. *Platelets*. 2022:1-9.

13. Zou L, Feng Y, Xu G, Jian W and Chao W. Splenic RNA and MicroRNA Mimics Promote Complement Factor B Production and Alternative Pathway Activation via Innate Immune Signaling. *Journal of immunology*. 2016;196:2788-98.

14. Zhang Z, Ohto U, Shibata T, Taoka M, Yamauchi Y, Sato R, Shukla NM, David SA, Isobe T, Miyake K and Shimizu T. Structural Analyses of Toll-like Receptor 7 Reveal Detailed RNA Sequence Specificity and Recognition Mechanism of Agonistic Ligands. *Cell Rep*. 2018;25:3371-3381 e5.

15. Lopez K, Suen A, Yang Y, Wang S, Williams B, Zhu J, Hu J, Fiskum G, Cross A, Kozar R, Miller C, Zou L and Chao W. Hypobaria Exposure Worsens Cardiac Function and Endothelial Injury in an Animal Model of Polytrauma: Implications for Aeromedical Evacuation. *Shock*. 2020;Publish Ahead of Print.

16. Naganathar S, De'Ath HD, Wall J and Brohi K. Admission biomarkers of trauma-induced secondary cardiac injury predict adverse cardiac events and are associated with plasma catecholamine levels. *J Trauma Acute Care Surg*. 2015;79:71-7.

LIST OF SYMBOLS, ABBREVIATIONS AND ACRONYMS

°C	degrees Celsius
%	percent
mg/kg	milligram(s) per kilogram
mL	milliliter(s)
mL/min	milliliter(s) per minute
mM	millimolar(s)
ng/mL	nanogram(s) per milliliter
pg/mL	picogram(s) per milliliter
µg/mL	microgram(s) per milliliter
µL/mL	microliter(s) per milliliter
g	gram(s)
h	hour(s)
d	day(s)

711 HPW/RHBAM	711th Human Performance Wing, Airman Systems Directorate, Airman Biosciences Division, Product Development Branch, Enroute Care Section
AE	Aeromedical Evacuation
AFRL	Air Force Research Laboratory
AKI	Acute kidney injury
ANOVA	Analysis of Variance
AST	Aspartate transferase
BAL	Bronchoalveolar lavage
BMDM	Bone marrow-derived macrophages
cDNA	Complementary DNA
cel-mir-39	*Caenorhabditis elegans* mir-39
CI	Confidence interval
CO	Cardiac output
CV	Coefficient of variant
CXCL-2	Chemokine CXC ligand-2
DEPC	Diethyl Pyrocarbonate
EC_{50}	Half maximal effective concentration
ELISA	Enzyme-Linked Immunosorbent Assay
ex-miRNA	Extracellular micro ribonucleic acid
FB	Factor B

FC	fold change
FDR	False Discovery Rate
FS	Fraction shortening
Fig.	Figure
GAPDH	Glyceraldehyde 3-phosphate dehydrogenase
H_2O	Water
H&E	Hematoxylin & eosin
HPLC	High-pressure liquid chromatography
HR	Heart rate
HRP	Horseradish peroxidase
IACUC	Institutional Animal Care and Use Committee
IED	Improvised explosion device(s)
IL-1β	Interleukin-1-beta
IL-6	Interleukin-6
KIM-1	Kidney injury molecule-1
LAX	Longitudinal axis
LV	Left ventricular
LVIDd	Left ventricular internal diameter end diastole
LVIDs	Left ventricular internal diameter end systole
min	Minutes
MIP-2	Macrophage inflammatory protein 2
miRNA	Micro ribonucleic acid
mRNA	Messenger ribonucleic acid
M-MLV	Moloney Murine Leukemia Virus Reverse Transcriptase
NaCl	Sodium chloride
NBF	Neutral Buffered Formalin
NGAL	Neutrophil gelatinase-associated lipocalin
PAGE	Polyacrylamide Gel Electrophoresis
PBS	Phosphate buffered saline
PCR	Polymerase chain reaction
piRNA	Piwi-interacting ribonucleic acid

PT	Polytrauma
qPCR	Quantitative real-time polymerase chain reaction
RE	Relative expression
RNA	Ribonucleic acid
RNASeq	Ribonucleic acid sequencing
rRNA	Ribosomal ribonucleic acid
SAX	Short axis
SDS	Sodium dodecyl-sulfate
SH	Sham
SMA	Superior mesenteric artery
ssRNA	Single strand ribonucleic acid
SV	Stroke volume
TBI	Traumatic brain injury
TBST	Tris buffered saline with 0.1% tween 20 detergent
TLR	Toll-like receptor
TLR3	Toll-like receptor 3
TLR7	Toll-like receptor 7
TMM	Trimmed mean of M-value
TNF-α	Tumor necrosis factor-alpha
tRNA	Transfer ribonucleic acid
U	Uridine(s)
UV	Ultraviolet
WT	Wild type